

# Substructure in the Circumstellar Disk around the Young Star AU Mic (GJ 803)

Michael C. Liu

Institute for Astronomy, University of Hawaii,  
2680 Woodlawn Drive, Honolulu, HI 96822, USA

E-mail: mliu@ifa.hawaii.edu

Accepted for publication in *Science*

August 4, 2004

**Keck adaptive optics imaging with a physical resolution of 0.4 AU resolves the inner (15–80 AU) disk of AU Mic (GJ 803), the nearest known scattered light disk to Earth. The inner disk is asymmetric and possesses a sharp change in structure at 35 AU. The disk also shows spatially localized enhancements and deficits at 25–40 AU separations. The overall morphology points to the influence of unseen larger bodies and resembles structures expected from recent planet formation. AU Mic is coeval with the archetypical debris disk system  $\beta$  Pic, and the similarities between their two disks point to synchronous disk evolution. Multiple indications of substructure appear to be common in circumstellar disks at an age of  $\approx 12$  Myr.**

## 1 Introduction

After dissipation of their primordial disks of gas and dust, many stars develop debris disks, which are composed solely of collisionally regenerated dust. Debris disks have been identified by their thermal emission at IR and sub-millimeter wavelengths (1, 2). Their spectral energy distributions (SEDs) convey only a limited information about the extant physical processes. In this regard, the large resolved disk around  $\beta$  Pic has been a goldmine for scrutinizing the structure, composition, and dynamics of a debris disk (e.g., (3); (4) and references therein; (5, 6, 7, 8, 9)). However, a broader understanding has been hampered by the small number of systems that are spatially resolved.

The newly discovered disk around the young star AU Mic (GJ 803) offers a promising opportunity to examine the debris disk phenomenon. This well-studied flare star is among the youngest known M dwarfs in the solar neighborhood, with an estimated age of  $12^{+8}_{-4}$  Myr (10, 11) and a distance of only  $9.94 \pm 0.13$  pc from Earth (12). A recent search of nearby young ( $\sim 10$ –50 Myr) stars identified AU Mic as a bright sub-mm source, possessing  $0.01 M_{\oplus}$  of cold (40 K) dust with a fractional luminosity of  $L_{dust}/L_{star} = 6 \times 10^{-4}$  (13). Follow-up *R*-band ( $0.65 \mu\text{m}$ ) coronagraphic imaging discovered that AU Mic has a large disk seen in scattered light (14), the closest such disk to Earth. The seeing-limited discovery images detected the disk as close to the star as the outer edge of the focal plane mask, which was  $5''$  (50 AU) in radius. Little is known about AU Mic’s disk inside of 50 AU, a scale which corresponds to edge of the classical Kuiper belt in our own solar system (15).

## 2 Observations

AU Mic was observed on 27–28 June 2004 UT using the adaptive optics (AO) system on the Keck II 10-m telescope (16) with the facility coronagraphic camera NIRC2 and the *H*-band ( $1.63 \mu\text{m}$ ) filter. Conditions were clear, and the AO-corrected images have a full width at half maximum (FWHM) of  $0.04''$  (0.4 AU). Photometric calibrations were based on IR standard stars (17) and 2MASS photometry of the star  $21''$  to the southwest of AU Mic. The edge-on disk of AU Mic is remarkably bright, noticeable in individual raw images. No similar features were seen in images of other stars obtained as a control sample.

A “roll subtraction” technique was developed to remove the point spread function (PSF) from the images, thereby enabling study of the inner disk against the bright glare of the central star (18). This technique is similar to that used for observing programs with the *Hubble Space Telescope* (19, 20). The AU Mic disk is detected in the Keck AO imaging from 15–80 AU in projected separation (Fig. 1). The disk midplane is resolved, with an observed FWHM of 2.0–2.5 AU inside of 50 AU. The innermost ( $<15$  AU) regions are dominated by PSF subtraction residuals and are inaccessible to study in this dataset.

## 3 Properties of the Inner Disk

The AU Mic disk shows two large-scale asymmetries. (1) The midplanes are different sizes. The outer isophotes of the SE side are  $\approx 10\%$  smaller than those of the NW side. (2) The disk midplanes are not aligned. From 2–5'' in radius, their position angles (PA) are  $129.3 \pm 0.8^\circ$  and  $311.4 \pm 1.0^\circ$ , as measured east of north. The relative tilt from the *H*-band data is  $2.1 \pm 1.3^\circ$ , consistent with the  $6 \pm 3^\circ$  tilt seen at *R*-band for the outer disk (14). Unlike the other asymmetries discussed in this paper, this tilt asymmetry can be explained by the intrinsic dust scattering properties (21), rather than a structural asymmetry in the disk.

The disk midplanes do not follow a constant position angle. Both midplanes curve slightly to the north, with a  $\approx 1^\circ$  change in orientation seen in the  $H$ -band imaging. This bowing is suggestive of an interaction between the disk and the local interstellar medium (22). However, the direction of AU Mic’s proper motion is nearly aligned with the disk midplane, which is not consistent with this idea. The bowing may reflect the internal dynamics of the disk.

The radial surface brightness profile  $f_\nu$  is well-described by a power law,  $f_\nu \propto r^\alpha$ , where  $r$  is the projected separation (Fig. 2). From 35–60 AU separation,  $\alpha = -4.4 \pm 0.4$  and  $-4.4 \pm 0.3$  for the SE and NW sides, respectively. These are somewhat steeper than the  $R$ -band measurements from 50–210 AU, which have slopes of  $-3.6$  to  $-3.9$  (14), though the different angular resolution of the two datasets impedes direct comparison (0.04'' for  $H$ -band, 1.1'' for  $R$ -band). In the innermost disk, there is a change in slope at 35 AU, with  $\alpha = -1.0 \pm 0.3$  and  $-1.4 \pm 0.3$  for the SE and NW sides, respectively, as measured from 20–35 AU separation. Also, there is an indication that the break occurs at slightly different radii for the two midplanes,  $\approx 32$  AU for the SE side and  $\approx 38$  AU for the NW side, pointing to a nonaxisymmetric structure.

In addition to the large-scale asymmetries, the Keck AO imaging reveals smaller-scale asymmetries in the disk at 25–40 AU, both radially and vertically. These features are spatially resolved, being broader than the PSF; they lie outside the region of significant PSF subtraction residuals; and they are consistent in independent subsets of the data. Because the disk is seen nearly edge-on, the true physical prominence of the substructure is diminished by the smooth component of the disk along the line of sight.

The most obvious substructure resides in the SE midplane (Figs. 1 and 3). The SE side contains at least two radial enhancements, one at 25 AU and another at 31 AU. There is also a relative deficit in the scattered light at 29 AU. The NW side shows an enhancement at 25 AU aligned with the SE feature at 25 AU, indicative of a limb-brightened ring of material. However, no other obvious counterparts for the SE features are seen in the NW side, indicating structures with non-zero eccentricity and/or incomplete azimuthal extent (e.g., clumps). Such nonaxisymmetric structures are most naturally explained by the dynamical influence of unseen planets (23, 24).

The disk also possesses vertical substructure (Fig. 4). The prominent SE lumps at 25 and 31 AU reside at different elevations. Furthermore, the NW side shows a local enhancement at 37 AU which is displaced from the inner midplane. The micron-sized dust grains responsible for the scattered light are removed by collisions and/or Poynting-Robertson drag on timescales shorter than the age of the star (14). Therefore, the observed vertical substructure may originate from the inclined ( $\gtrsim 1^\circ$ ) orbits of larger unseen bodies, either the parent bodies which collisionally produce the dust or planets which gravitationally perturb the dust.

## 4 Comparing Disk Structure: AU Mic vs $\beta$ Pic

The debris disk archetype  $\beta$  Pic is the best-studied spatially resolved disk system. Many of the structural features present in the  $\beta$  Pic disk are also found in the AU Mic disk:

(1) Both disks have unequal-sized midplanes. In the case of  $\beta$  Pic, the NE side is larger than the SW side (25, 21), an effect which has been attributed to eccentricity perturbations driven by a substellar companion (26).

(2) The surface brightness profiles for the  $\beta$  Pic and AU Mic disks are similar, with steep outer profiles ( $\alpha \approx -4$  to  $-5$ ) and a strong flattening ( $\Delta\alpha \approx 2 - 3$ ) in the inner profile. For  $\beta$  Pic, the profile changes markedly inside of 100 AU compared to the outer disk (25, 21, 19). For AU Mic, the change occurs at 35 AU.

The steep slope of the  $\beta$  Pic outer disk has been modeled as dust originating from an inner collisional planetesimal disk and then radiatively driven outwards ( (27); cf., (28)). The strong flattening at 100 AU demarcates the outer extent of the  $\beta$  Pic planetesimal disk. By analogy, the similar flattening of the AU Mic profile suggests a planetesimal disk of 35 AU extent. This value is consistent with the  $\approx 17$  AU inner radius inferred from the IR/sub-mm SED (13). And taken together, the data suggest that AU Mic's planetesimal disk is restricted to  $\approx 17-35$  AU in radius.

The factor of 3 difference in the inferred sizes of the underlying planetesimal disks can be understood in the context of different agglomeration rates. The time scale for planetesimal growth scales as  $t \propto P/\Sigma$ , where  $P$  is the orbital period and  $\Sigma$  is the surface density (29). For a disk profile of  $\Sigma \propto \Sigma_0 a^{-3/2}$ , the growth time scale is then  $t \propto a^3/(\Sigma_0 M_\star^{1/2})$ , i.e., strongly dependent on the orbital radius  $a$ . The two stars are coeval, with a factor of 4 difference in stellar mass. Assuming the difference in the total disk masses is reflected in the factor of 10 difference in the sub-mm emitting dust masses (30, 13), planetesimal growth should have proceeded to  $\sim 2.7\times$  larger radii for  $\beta$  Pic compared to AU Mic, in accord with the observational estimates.

(3) The  $\beta$  Pic disk exhibits small-scale structures in its inner disk which are radially confined and vertically displaced (8), similar to the AU Mic disk. These features are naturally explained by radially localized structures in the dust with non-zero eccentricities and inclinations (e.g., rings, clumps, and gaps), perhaps arising from resonant interactions of multiple planets (31). The  $\beta$  Pic disk also displays a prominent inner warp (5, 19), with a  $3-4^\circ$  tilt relative to the outer disk. Such a strong warp is not seen in the AU Mic disk, though its detectability would depend on its radial extent and orientation to the line of sight.

## 5 Evolutionary Context

Since its discovery, the singular nature of the large scattered light disk around  $\beta$  Pic has raised the question of whether the system represents a typical phase in early disk evolution (4, 32) or an anomalous occurrence, e.g., caused by the gravitational perturbation of a passing star (6). The discovery and characterization of the coeval AU Mic disk demonstrate that a common phase in disk evolution involves optically thin, asymmetric, bright scattered-light disks with multiple indications of substructure. Given that AU Mic and  $\beta$  Pic are members of the same moving group (10, 11), the high degree of similarity between these two disks suggests synchronous evolution has occurred.

Dust with sufficient optical depth to produce detectable scattered light spans a large range in radius around  $\beta$  Pic and AU Mic, from as close as  $\approx 15$  AU out to hundreds of AU. This is in contrast to older ( $\gtrsim 200$  Myr) debris disk systems, where the dust is confined to ring-like structures detected in sub-mm thermal emission (33, 34) but not in scattered light (35, 36). Recent simulations of evolving planetesimal disks are in accord with this observed morphological transformation from young dusty disks to old dusty rings (37). However, the young ( $\sim 8$  Myr) A star HR 4796A has its scattered light confined to a single bright ring (38), as opposed to a large disk, so stellar age cannot be the only factor governing disk morphology.

The spatially localized enhancements and deficits found in the AU Mic disk resemble the expected signposts of recent and/or ongoing planet formation in young disks. Simulations of planet formation by agglomeration find that bright rings of dust arise from gravitational stirring of planetesimals by recently formed planets of  $\gtrsim 1000$  km radius (39, 37). Dark gaps occur where the dust has been dynamically removed by planets or represent regions shadowed by interior rings which are optically thick. In this interpretation, the multiple structures present in the AU Mic disk argue that planets massive enough to induce significant gravitational stirring form contemporaneously over a range of radii.

Finally, the stellar masses of  $\beta$  Pic ( $2 M_{\odot}$ ) and AU Mic ( $0.5 M_{\odot}$ ) straddle that of solar-mass stars. Hence, scrutiny of these two well-resolved disks may provide a window into the early solar system. The young Kuiper belt was about a factor of 100 more massive than its current state (40); its fractional dust luminosity would have been around  $10^{-3}$  to  $10^{-5}$  (15, 41), comparable to the  $\beta$  Pic and AU Mic disks. This Keck AO study reveals that multiple dynamical substructures are common to optically thin disks at ages of  $\approx 12$  Myr. These structures may also reflect the dynamics that were active in the young Kuiper belt.

## References and Notes

1. D. E. Backman, F. Paresce, *Protostars and Planets III* (1993), p. 1253.
2. A.-M. Lagrange, D. E. Backman, P. Artymowicz, *Protostars and Planets IV* p. 639 (2000).

3. B. A. Smith, R. J. Terrile, *Science* **226**, 1421 (1984).
4. P. Artymowicz, *Annual Review of Earth and Planetary Sciences* **25**, 175 (1997).
5. D. Mouillet, J. D. Larwood, J. C. B. Papaloizou, A. M. Lagrange, *MNRAS* **292**, 896 (1997).
6. P. Kalas, J. Larwood, B. A. Smith, A. Schultz, *ApJ* **530**, L133 (2000).
7. A. J. Weinberger, E. E. Becklin, B. Zuckerman, *ApJ* **584**, L33 (2003).
8. Z. Wahhaj, *et al.*, *ApJ* **584**, L27 (2003).
9. A. Brandeker, R. Liseau, G. Olofsson, M. Fridlund, *A&A* **413**, 681 (2004).
10. D. Barrado y Navascués, J. R. Stauffer, I. Song, J.-P. Caillault, *ApJ* **520**, L123 (1999).
11. B. Zuckerman, I. Song, M. S. Bessell, R. A. Webb, *ApJ* **562**, L87 (2001).
12. M. A. C. Perryman, *et al.*, *A&A* **323**, L49 (1997).
13. M. C. Liu, B. C. Matthews, J. P. Williams, P. G. Kalas, *ApJ* **608**, 526 (2004).
14. P. Kalas, M. C. Liu, B. C. Matthews, *Science* **303**, 1990 (2004).
15. D. C. Jewitt, J. X. Luu, *Protostars and Planets IV* p. 1201 (2000).
16. P. Wizinowich, *et al.*, *PASP* **112**, 315 (2000).
17. S. E. Persson, D. C. Murphy, W. Krzeminski, M. Roth, M. J. Rieke, *AJ* **116**, 2475 (1998).
18. Materials and methods are available as supporting material on *Science Online*.
19. S. R. Heap, *et al.*, *ApJ* **539**, 435 (2000).
20. G. Schneider, M. D. Silverstone, *High-Contrast Imaging for Exo-Planet Detection. Edited by Alfred B. Schultz. Proceedings of the SPIE, Volume 4860, pp. 1-9 (2003)*. (2003), pp. 1–9.
21. P. Kalas, D. Jewitt, *AJ* **110**, 794 (1995).
22. P. Artymowicz, M. Clampin, *ApJ* **490**, 863 (1997).
23. J. Liou, H. A. Zook, *AJ* **118**, 580 (1999).
24. L. M. Ozernoy, N. N. Gorkavyi, J. C. Mather, T. A. Taidakova, *ApJ* **537**, L147 (2000).
25. D. A. Golimowski, S. T. Durrance, M. Clampin, *ApJ* **411**, L41 (1993).
26. D. P. Whitmire, J. J. Matese, L. J. Tomley, *A&A* **203**, L13 (1988).

27. J. C. Augereau, R. P. Nelson, A. M. Lagrange, J. C. B. Papaloizou, D. Mouillet, *A&A* **370**, 447 (2001).
28. A. Lecavelier Des Etangs, A. Vidal-Madjar, R. Ferlet, *A&A* **307**, 542 (1996).
29. J. J. Lissauer, *Icarus* **69**, 249 (1987).
30. I. Sheret, W. R. F. Dent, M. C. Wyatt, *MNRAS* **348**, 1282 (2004).
31. E. W. Thommes, J. J. Lissauer, *ApJ* **597**, 566 (2003).
32. M. Jura, *et al.*, *ApJ* **505**, 897 (1998).
33. J. S. Greaves, *et al.*, *ApJ* **506**, L133 (1998).
34. W. S. Holland, *et al.*, *Nature* **392**, 788 (1998).
35. B. A. Smith, J. W. Fountain, R. J. Terrile, *A&A* **261**, 499 (1992).
36. P. Kalas, D. Jewitt, *AJ* **111**, 1347 (1996).
37. S. J. Kenyon, B. C. Bromley, *AJ* **127**, 513 (2004).
38. G. Schneider, *et al.*, *ApJ* **513**, L127 (1999).
39. S. J. Kenyon, B. C. Bromley, *ApJ* **577**, L35 (2002).
40. S. A. Stern, J. E. Colwell, *AJ* **114**, 841 (1997).
41. C. Dominik, G. Decin, *ApJ* **598**, 626 (2003).
42. It is a pleasure to thank Eugene Chiang, Greg Herczeg, Mike Jura, Paul Kalas, John Krist, Jeff Linsky, and Bruce Macintosh for enlightening discussions. We are very grateful to Antonin Bouchez, David LeMignant, Randy Campbell, Peter Wizinowich, and the staff of Keck Observatory for their assistance with the observations. This research has made use of the NASA/IPAC, 2MASS, and SIMBAD databases. We acknowledge support from NSF grant AST04-07441 and NASA grant HST-GO-09845.01-A.

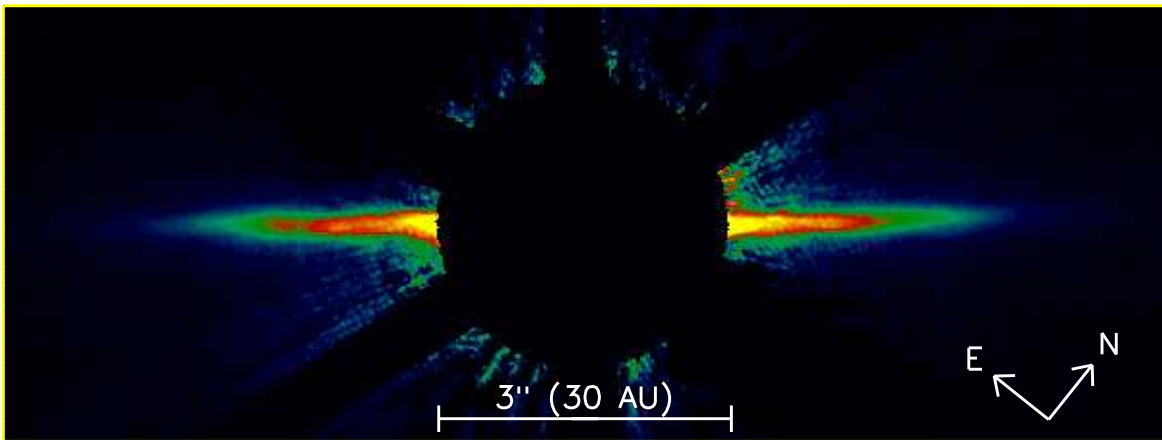


Figure 1: *H*-band ( $1.63 \mu\text{m}$ ) image of the AU Mic dust disk obtained with the Keck II telescope. The image is  $12''$  (119 AU) wide and  $4.5''$  (45 AU) high. A software mask has been applied to block the PSF subtraction residuals around the six diffraction spikes and the central  $1.5''$  (15 AU) radius region.



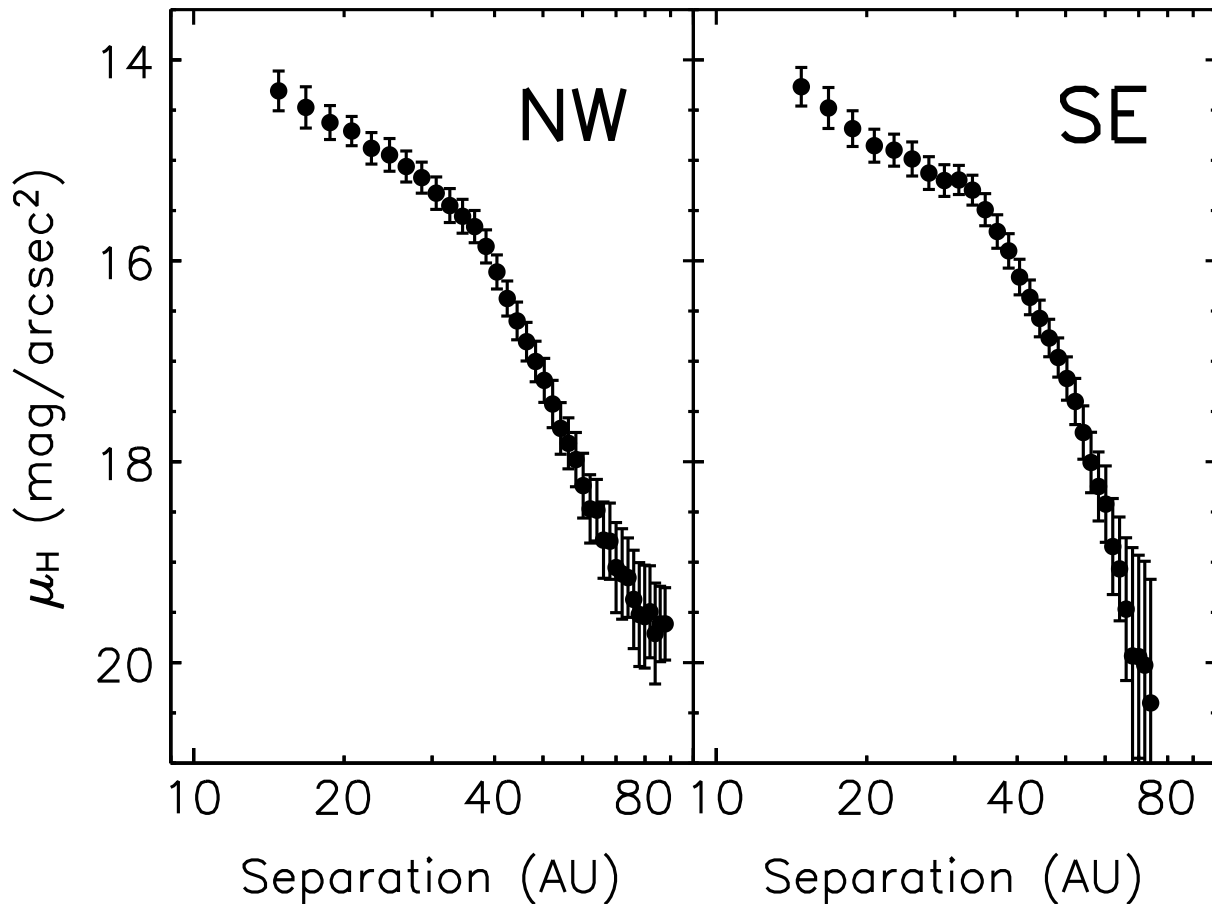


Figure 2:  $H$ -band ( $1.63 \mu\text{m}$ ) surface brightness profile of the AU Mic disk midplane derived from a photometry aperture  $0.6''$  wide in the direction perpendicular to the midplane. The NW side of the disk is larger than the SE side. A break in the surface brightness profile is seen at 35 AU.

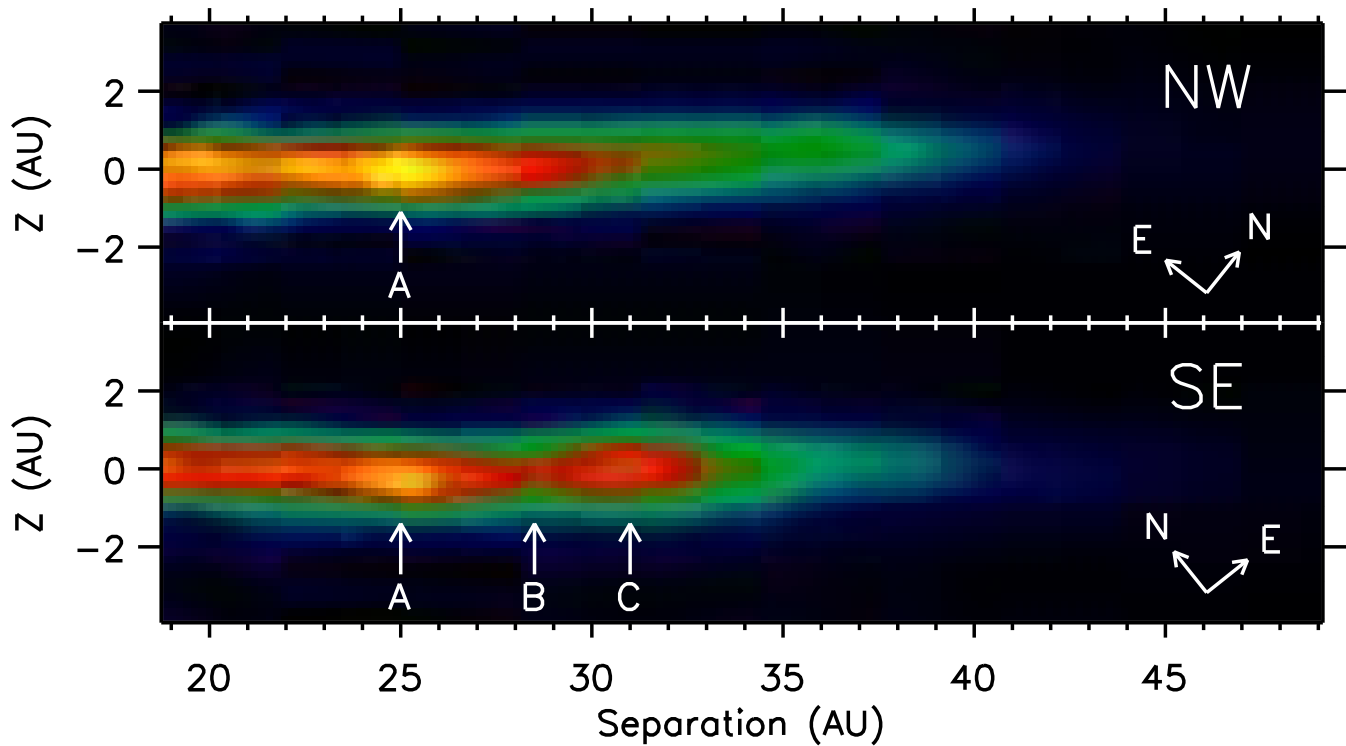


Figure 3: Radial substructure in the AU Mic disk. The SE data have been mirrored about the axis perpendicular to the disk midplane. To highlight the substructure, each pixel has been multiplied by its distance from the star, in order to compensate for the overall decrease in disk flux with radius. The data have been gaussian smoothed to the image resolution of  $0.04''$  (0.4 AU). The data are oriented with the SE midplane horizontal; the small relative tilt of the NW midplane can be seen.

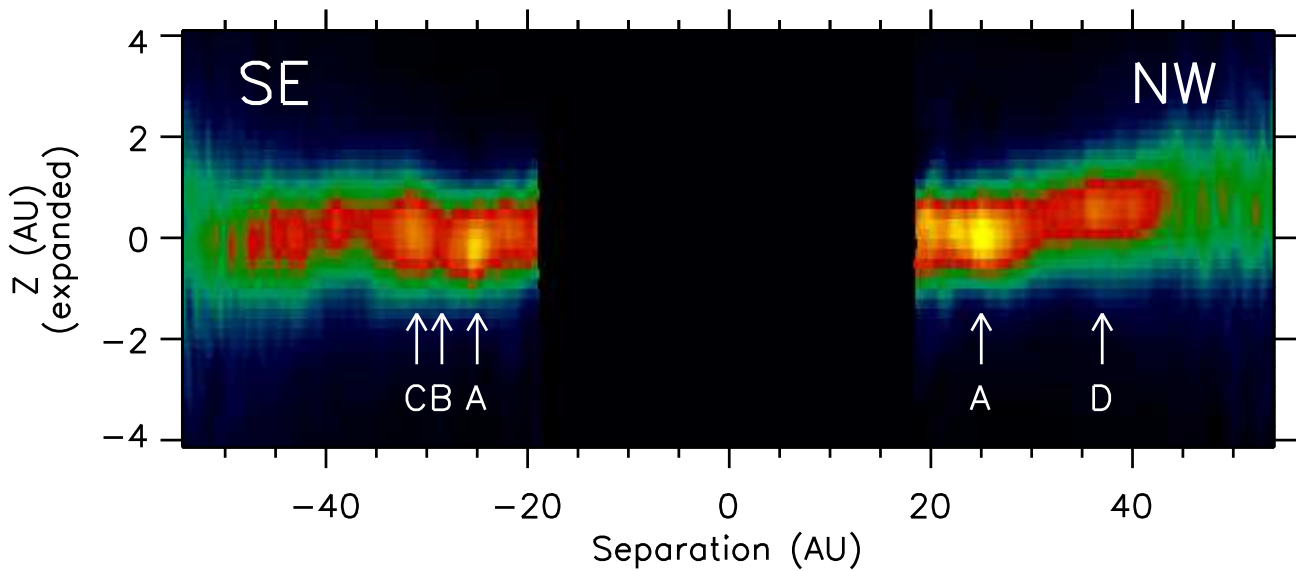


Figure 4: Vertical substructure in the AU Mic disk. The plot's vertical axis has been expanded by a factor of 5. The NW concentration at 25 AU is aligned with its SE counterpart, but the strong features at 25 and 31 AU in the SE midplane reside at different heights. The elevated NW structure at 37 AU has no clear counterpart. To show the structure over a wide range of separations, the disk flux has been normalized by the radial surface brightness profile in Fig. 2 (different than the normalization used for Fig. 3). The data have been gaussian smoothed to the image resolution of  $0.04''$  (0.4 AU). The image orientation is the same as in Fig. 1.

## SUPPORTING ONLINE MATERIAL: Observing and Data Reduction Methods

A combination of coronagraphy and a “roll subtraction” observing technique were employed to maximize the dynamic range and contrast of the observation, thereby enabling study of the scattered light disk around AU Mic against the bright glare of the central star.

The facility near-IR camera NIRC2 is equipped with a variety of translucent circular masks in its first focal plane. The 2'' diameter mask was used for the AU Mic observations. The mask greatly reduced the light from the PSF's central region, thereby avoiding detector saturation and allowing for longer integrations. The net result was to increase the dynamic range of the instrument and the observing efficiency. Both the wide and narrow camera optics in NIRC2 were used, which provide pixel scales of  $39.69 \pm 0.05$  mas pixel<sup>-1</sup> and  $9.94 \pm 0.05$  mas pixel<sup>-1</sup>, respectively.

A “roll subtraction” technique was developed to remove the PSF, similar to methods used for observing programs with the *Hubble Space Telescope*. Taking advantage of the fact that Keck is an alt-azimuth telescope, images were obtained such that the telescope pupil orientation, and hence the Keck PSF, remained fixed relative to the detector while the orientation of the sky rotated. Thus, the orientation of AU Mic's disk changed on the detector as the star moved across the sky. Individual images were subtracted from each other to remove the PSF, but leaving the disk. The optimal scaling between two images was determined by minimizing the residuals in an annular region of high PSF flux, with the scaling factors being at most a few percent.

Individual roll-subtracted images were then aligned and rotated to a common orientation; the diffraction spikes and the negative counterpart images from the roll subtraction were masked; and a final mosaic was constructed by median averaging. One potential limitation of this method is that the disk may overlap and thereby self-subtract if the amount of rotation between the two images is small. This effect was avoided by observing AU Mic over a wide range of sky orientations, resulting in 30–40° of rotation between subtracted pairs of images.

Photometry errors are dominated by the residuals from roll subtraction. To quantify these at each radius, we measured the scatter in photometry from apertures placed at arbitrary position angles and using independent subsets of the data. These errors were added in quadrature to the errors in the photometric calibration. The resulting total errors are plotted in Fig. 2.